Pergamon

0956-7151(94)E0152-7

Acta metall. mater. Vol. 42, No. 11, pp. 3827–3836, 1994

0956-7151/94 $7.00 + 0.00

SHEAR INDUCED TRANSFORMATION TOUGHENING IN CERAMICS

N. SIMHA and L. TRUSKINOVSKY

Department of Aerospace Engineering and Mechanics, University of Minnesota, Minneapolis, MN 55455, U.S.A.

(Received 6 February 1994)

Abstract—There is experimental evidence that the tetragonal to monoclinic transformation in zirconia (ZrO_2) can be triggered not only by hydrostatic pressure but also by shear stresses. In this paper we consider the implications of a transformation criterion which depends on both mean stress and shear stress on transformation toughening in ceramics reinforced with zirconia inclusions. We treat zirconia toughened ceramics (ZTC) as dilute composites of randomly oriented inclusions in an elastic matrix and develop the constitutive model for the composite from the behaviour of single inclusions by orientation averaging. We then study quasistatic crack propagation and predict the transformation zone, distribution of transformed inclusions and toughness enhancement.

1. INTRODUCTION

It has been observed that the fracture toughness of certain ceramics (typically 2–4 MPa$\sqrt{m}$) increases when inclusions of zirconia (ZrO_2) are present and toughness values as high as 18–20 MPa$\sqrt{m}$ [1, 2] have been achieved for zirconia toughened ceramics (ZTC). This increase is due to the tetragonal to monoclinic (t→m) transformation of zirconia, induced by stresses around a crack tip. Since the discovery of transformation toughening by Garvie *et al.* [3], it has been extensively studied and a new generation of strong and tough ceramics (e.g. PSZ, TZP, CSZ, ZTA) have emerged (see [4–6] for a review).

Although the t→m transformation is accompanied by both dilatation of about 4% and a shear strain of about 16%, most of the experimental work on phase stability of zirconia was done under hydrostatic loading [7–10]. Since inclusions are usually twinned [11, 12], most theoretical studies have also neglected the shear aspect of this transformation, assuming that it is triggered only by mean stress [13–16]. However recent experiments on Mg-PSZ, Ce-TZP [17–19] have shown that the t→m transformation may be triggered by shear stress alone. There are several theoretical studies of the effect of shear on transformation toughening which explore the implications of different phenomenological transformation criteria for polycrystals or composites [17, 20, 21]. Recently Budiansky and Truskinovsky [22] have suggested a simple constitutive model for single-crystal zirconia which is consistent with experimental pressure–temperature phase diagram of zirconia and results in a transformation criterion depending on both mean stress and shear stress. In this paper we adopt this model for zirconia inclusions, develop a constitutive model for ZTC and investigate its implications on transformation toughening.

We treat ZTC as a dilute composite of spherical zirconia inclusions in an elastic matrix. In experimental samples the inclusions are on the scale of fractions of a micrometer [6]. We therefore assume that a representative material point in the composite contains randomly oriented inclusions which do not interact. Each inclusion is then viewed as a constrained inclusion in an infinite elastic matrix. The constitutive behaviour of the composite is obtained by orientation averaging, a method that has been successfully used in the closely related slip theory of plasticity [23] as well as in other theories of composite materials [24]. We then consider steady quasistatic crack propagation in a ZTC and predict the distribution of transformed inclusions in the transformation zone. Following [13–15] we evaluate toughening due to transformed inclusions by finding the transformation induced stress intensity factor.

In Section 2 we describe the constitutive relations for single-crystal zirconia and for a constrained zirconia inclusion. In Section 3 we discuss constitutive behaviour of the composite. In Section 4 we find the transformation zone around a propagating crack, calculate the resulting toughening enhancement and compare our predictions with those based on a model with purely mean stress transformation criterion [13, 14].

2. CONSTITUTIVE MODEL

In the absence of stresses, tetragonal phase of zirconia is stable at high temperatures while monoclinic phase is stable at low temperatures and the

t→m transition exhibits considerable hysterisis [7]. Figure 1 is a sketch of an experimental phase diagram of single-crystal zirconia exhibiting the linear dependence of critical transformation pressure on temperature (see [8–10]).

In this paper single-crystal zirconia is considered to be a nonlinear elastic material with a non-convex energy that has multiple wells corresponding to the tetragonal and monoclinic phases. Let $\bar{\sigma}$ be the mean stress and $\bar{\theta}$ the dilatation (see Fig. 2). Let $\bar{\tau}$ be the shear in one of the tetragonal planes and $\bar{\gamma}$ the corresponding engineering shear strain. We adopt the simple two parameter constitutive model of Budiansky and Truskinovsky [22] and take the free energy F to be a polynomial in dilatation $\bar{\theta}$ and shear strain $\bar{\gamma}$

$$F(\bar{\theta},\bar{\gamma})=\tfrac{1}{2}\kappa\bar{\theta}^2+\tfrac{1}{2}G\bar{\gamma}^2-C\bar{\theta}\bar{\gamma}^2+\tfrac{1}{4}B\bar{\gamma}^4+\tfrac{1}{6}D\bar{\gamma}^6, \quad (1)$$

where κ is the bulk modulus of the tetragonal phase and G, C, B, D are constants which are determined from experimental phase diagram of single-crystal zirconia (Fig. 1) and by using the transformation strain. In equation (1) the quadratic terms account for the linear theory of elasticity, the cubic term couples the shear strain and dilatation while the remaining terms guarantee existence of two monoclinic variants. For equilibrium considerations in the case of hydrostatic loading $\bar{\sigma}$ with a superimposed shear stress $\bar{\tau}$ (see Fig. 2), the relevant potential energy is

$$\Phi(\bar{\theta},\bar{\gamma})=F(\bar{\theta},\bar{\gamma})-\bar{\sigma}\bar{\theta}-\bar{\tau}\bar{\gamma}. \quad (2)$$

Restricting to the class of homogeneous deformations, the conditions for equilibrium are

$$\frac{\partial\Phi}{\partial\bar{\theta}}=\frac{\partial\Phi}{\partial\bar{\gamma}}=0. \quad (3)$$

In [22] tetragonal–monoclinic transition is attributed to the instability that results from the softening of a shear modulus, i.e.

$$\text{Det}\begin{bmatrix}\frac{\partial\bar{\sigma}}{\partial\bar{\theta}} & \frac{\partial\bar{\sigma}}{\partial\bar{\gamma}}\\ \frac{\partial\bar{\tau}}{\partial\bar{\theta}} & \frac{\partial\bar{\tau}}{\partial\bar{\gamma}}\end{bmatrix}=\kappa\frac{\partial\bar{\tau}}{\partial\bar{\gamma}}\Big|_{\bar{\sigma}}=0, \quad \kappa>0 \quad (4)$$

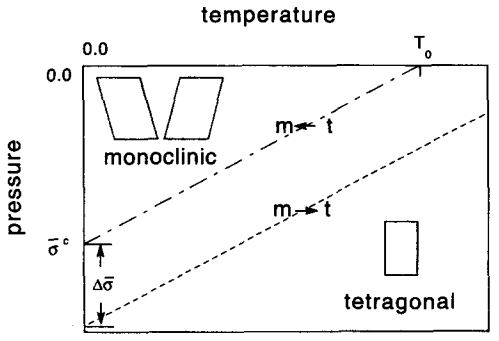

Fig. 1. Sketch of an experimental phase diagram for single-crystal zirconia. Tetragonal to monoclinic transition occurs on line t→m, while monoclinic to tetragonal transition occurs on line m→t.

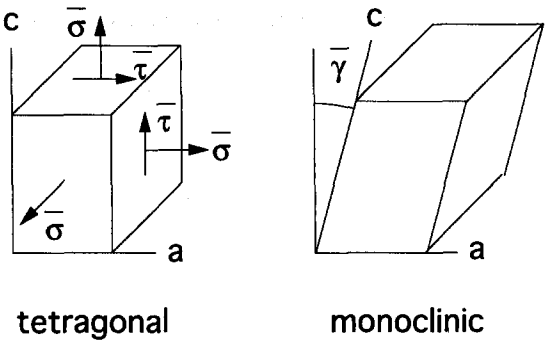

Fig. 2. Stresses which trigger transformation (mean stress $\bar{\sigma}$ and a shear stress $\bar{\tau}$). The monoclinic variants can be obtained by axial extensions and shearing a rectangular face of the tetragonal unit cell.

where $\bar{\sigma}(\bar{\theta},\bar{\gamma})$ and $\bar{\tau}(\bar{\theta},\bar{\gamma})$ are found by solving equations (3). At zero temperature and zero shear stress, t→m transformation occurs at a critical mean stress $\bar{\sigma}^c$ resulting in a transformation dilatation $\bar{\theta}_T$ and a transformation shear strain $\bar{\gamma}_T$, while the m→t occurs at a mean stress $\bar{\sigma}^c-\Delta\bar{\sigma}$ (see Fig. 1). By using the values of $\bar{\sigma}^c\,(<0)$, $\Delta\bar{\sigma}$, $\bar{\theta}_T$ and $\bar{\gamma}_T$ and equations (3) and (4), constants G, C, B, D in equation (1) can be evaluated explicitly (see [22] for details). Then the free energy is

$$F(\bar{\theta},\bar{\gamma})=\frac{1}{2}\kappa\bar{\theta}^2+(\bar{\sigma}^c-\kappa\bar{\theta})\bar{\theta}_T\left(\frac{\bar{\gamma}}{\bar{\gamma}_T}\right)^2+\frac{\kappa\bar{\theta}_T^2}{2}\left(\frac{\bar{\gamma}}{\bar{\gamma}_T}\right)^4-2\Delta\bar{\sigma}\bar{\theta}_T\left(\frac{\bar{\gamma}}{\bar{\gamma}_T}\right)^4\times\left[1-\frac{2}{3}\left(\frac{\bar{\gamma}}{\bar{\gamma}_T}\right)^2\right] \quad (5)$$

and the conditions for equilibrium [equations (3)] are

$$\frac{\bar{\sigma}}{\kappa\bar{\theta}_T}=\frac{\bar{\theta}}{\bar{\theta}_T}-\left(\frac{\bar{\gamma}}{\bar{\gamma}_T}\right)^2, \quad (6)$$

$$\frac{\bar{\gamma}_T\bar{\tau}}{|\bar{\sigma}^c|\bar{\theta}_T}=2\frac{\bar{\gamma}}{\bar{\gamma}_T}\left\{\frac{4\Delta\bar{\sigma}}{|\bar{\sigma}^c|}\left[\left(\frac{\bar{\gamma}}{\bar{\gamma}_T}\right)^4-\left(\frac{\bar{\gamma}}{\bar{\gamma}_T}\right)^2\right]-\frac{\bar{\sigma}}{|\bar{\sigma}^c|}+\frac{\bar{\sigma}^c}{|\bar{\sigma}^c|}\right\}. \quad (7)$$

Now, following Budiansky and Truskinovsky [22], consider a spherical inclusion in an infinite isotropic linear elastic matrix. Let the matrix be subjected to homogeneous far-field hydrostatic stress $\bar{\sigma}^\infty$ and shear stress $\bar{\tau}^\infty$ and suppose that the inclusion is oriented in such a way that $\bar{\tau}^\infty$ is aligned with $\bar{\tau}$. Stresses $(\bar{\sigma},\bar{\tau})$ and strains $(\bar{\theta},\bar{\gamma})$ inside the inclusion are assumed to be uniform and related through equations (6) and (7). Then the exact Eshelby–Hill relations [25, 26] can be written as

$$\bar{\sigma}^\infty-\eta\bar{\sigma}=\kappa(1-\eta)\bar{\theta}$$

$$\bar{\tau}^\infty-\zeta\bar{\tau}=\kappa\frac{3(1-2\nu)}{2(1+\nu)}(1-\zeta)\bar{\gamma} \quad (8)$$

where ν is the Poisson's ratio and the Eshelby parameters are

$$\eta = \frac{(1+\nu)}{3(1-\nu)}, \quad \zeta = \frac{2(4-5\nu)}{15(1-\nu)};$$

the bulk modulus of the matrix κ has been assumed to be the same as that of the inclusion. Since the control parameters are now $\tilde{\sigma}^\infty$ and $\tilde{\tau}^\infty$, the instability condition for the constrained inclusion is

$$\left.\frac{\partial \tilde{\tau}^\infty}{\partial \bar{\gamma}}\right|_{\tilde{\sigma}^\infty} = 0. \tag{9}$$

Equation (9) is analogous to equation (4). Eliminating $\bar{\sigma}$ and $\bar{\tau}$ in equation (8) one can relate far-field stresses $\tilde{\sigma}^\infty$ and $\tilde{\tau}^\infty$ directly to $\bar{\theta}$ and $\bar{\gamma}$ (see [22] for details)

$$\frac{\tilde{\sigma}^\infty}{\kappa\tilde{\theta}_T} = \frac{\bar{\theta}}{\tilde{\theta}_T} - \left(\frac{\bar{\gamma}}{\tilde{\gamma}_T}\right)^2 \tag{10}$$

$$\frac{\eta\tilde{\gamma}_T\tilde{\tau}^\infty}{\zeta|\tilde{\sigma}^c|\tilde{\theta}_T} = 2\frac{\bar{\gamma}}{\tilde{\gamma}_T}\left\{\frac{4\Delta\tilde{\sigma}}{|\tilde{\sigma}^c|}\left[\left(\frac{\bar{\gamma}}{\tilde{\gamma}_T}\right)^4 - \left(\frac{\bar{\gamma}}{\tilde{\gamma}_T}\right)^2\right] - \frac{\tilde{\sigma}^\infty}{|\tilde{\sigma}^c|} + \frac{\tilde{\sigma}^c}{|\tilde{\sigma}^c|}\right\} \tag{11}$$

where

$$\tilde{\sigma}^c = \tilde{\sigma}^c + \frac{9\kappa\Delta\tilde{\sigma}(7-5\nu)(1-\nu)(1-2\nu)}{2\tilde{\theta}_T(1+\nu)(4-5\nu)[6\Delta\tilde{\sigma}(1-\nu) - \kappa\tilde{\theta}_T(1-2\nu)]}\tilde{\gamma}_T^2 \tag{12}$$

$$\tilde{\gamma}_T = \sqrt{1 - \frac{\kappa\tilde{\theta}_T(1-2\nu)}{6\Delta\tilde{\sigma}(1-\nu)}}\,\bar{\gamma}_T \tag{13}$$

$$\tilde{\theta}_T = \frac{1+\nu}{3(1-\nu)}\bar{\theta}_T - \frac{\kappa(1-2\nu)(1+\nu)}{18\Delta\tilde{\sigma}(1-\nu)^2}\bar{\theta}_T^2 \tag{14}$$

$$\Delta\tilde{\sigma} = \left[1 - \frac{\kappa\tilde{\theta}_T(1-2\nu)}{6\Delta\tilde{\sigma}(1-\nu)}\right]^2 \Delta\tilde{\sigma}. \tag{15}$$

It can be shown from equations (10) and (11) that for $\tilde{\tau}^\infty = 0$, t→m transition occurs at a far-field mean stress $\tilde{\sigma}^\infty = \tilde{\sigma}^c$ and is accompanied by transformation dilatation $\tilde{\theta}_T$ and transformation shear strain $\tilde{\gamma}_T$. On the other hand m→t transition occurs at $\tilde{\sigma}^\infty = \tilde{\sigma}^c - \Delta\tilde{\sigma}$. We notice that the right hand sides of equations (10) and (11) can be obtained by replacing $\{\bar{\theta}_T, \bar{\gamma}_T, \bar{\sigma}, \bar{\sigma}^c, \Delta\bar{\sigma}\}$ with $\{\tilde{\theta}_T, \tilde{\gamma}_T, \tilde{\sigma}^\infty, \tilde{\sigma}^c, \Delta\tilde{\sigma}\}$ respectively in the right hand side of equations (6) and (7). We rewrite the conditions for equilibrium of a constrained inclusion [equations (10) and (11)], in non-dimensional variables

$$\sigma^\infty = \frac{\tilde{\sigma}^\infty}{|\tilde{\sigma}^c|}, \quad \tau^\infty = \frac{\tilde{\tau}^\infty}{|\tilde{\sigma}^c|}, \quad \theta = \frac{\bar{\theta}}{\tilde{\theta}_T}, \quad \gamma = \frac{\bar{\gamma}}{\tilde{\gamma}_T}, \tag{16}$$

to obtain

$$\lambda\sigma^\infty = \theta - \gamma^2 \tag{17}$$

$$\tau^\infty = 2R\gamma\{4\omega(\gamma^2-1)\gamma^2 - \sigma^\infty + 1\} \tag{18}$$

where constants λ, ω and R are defined as

$$\lambda = \frac{|\tilde{\sigma}^c|}{\kappa\tilde{\theta}_T}, \quad \omega = \frac{\Delta\tilde{\sigma}}{|\tilde{\sigma}^c|}, \quad R = \frac{\zeta\tilde{\theta}_T}{\eta\tilde{\gamma}_T}. \tag{19}$$

The constant λ characterises the critical mean stress required for t→m transition and ω is a measure of the hysterisis, while R characterises the effective transformation shear strain.

We rewrite equation (9) in non-dimensional form as

$$\sigma^\infty = 1 + 4\omega\gamma^2(5\gamma^2 - 3). \tag{20}$$

To obtain an explicit representation for the stability diagram we simplify equation (18) using (20) to get

$$\tau^\infty = \frac{8R}{5}\gamma[1 - \sigma^\infty - 2\omega\gamma^2] \tag{21}$$

and solving equation (20) for γ we obtain

$$\gamma^\pm = \left\{\frac{3}{10}\left[1 \pm \sqrt{1 + \frac{5}{9\omega}(\sigma^\infty - 1)}\right]\right\}^{1/2}. \tag{22}$$

Let's define

$$f(\sigma^\infty) = \frac{8R}{5}\sqrt{\left\{\frac{3}{10}\left[1 - \sqrt{1 + \frac{5}{9\omega}(\sigma^\infty - 1)}\right]\right\}} \times \left[1 - \sigma^\infty - 2\omega\left\{\frac{3}{10}\left[1 - \sqrt{1 + \frac{5}{9\omega}(\sigma^\infty - 1)}\right]\right\}\right], \tag{23}$$

$$b(\sigma^\infty) = \frac{8R}{5}\sqrt{\left\{\frac{3}{10}\left[1 + \sqrt{1 + \frac{5}{9\omega}(\sigma^\infty - 1)}\right]\right\}} \times \left[1 - \sigma^\infty - 2\omega\left\{\frac{3}{10}\left[1 + \sqrt{1 + \frac{5}{9\omega}(\sigma^\infty - 1)}\right]\right\}\right]. \tag{24}$$

Then it follows from equations (21) and (22) that tetragonal phase becomes unstable when $\tau^\infty = \pm f(\sigma^\infty)$, while monoclinic phase becomes unstable when $\tau^\infty = \pm b(\sigma^\infty)$.

To illustrate these relations one has to fix the values of the non-dimensional parameters λ, ω and R. For the rest of the paper we shall take $\tilde{\sigma}^c = 0.5$ GPa [17], $\Delta\tilde{\sigma} = 0.6$ GPa [8], $\kappa = 170$ GPa [27], $\nu = 0.3$ [6] and $\tilde{\theta}_T = 0.04$. Instead of fixing the effective shear strain $\tilde{\gamma}_T$, we shall consider it as a parameter. In fact, since inclusions are usually twinned upon transformation, the effective shear strain $\tilde{\gamma}_T$ is often considered to be zero [13–16]. This gives $\lambda = 0.07$, $\omega = 1.2$ and $R = \infty$. In this paper we assume that $\tilde{\gamma}_T > 0$ but small, neglect the influence of $\tilde{\gamma}_T$ on λ and ω (second order) and consider different values for R.

Figure 3 shows phase diagrams for a constrained inclusion for different R. Phase diagrams are symmetric about $\tau^\infty = 0$, hence only $\tau^\infty = f(\sigma^\infty)$ and $\tau^\infty = b(\sigma^\infty)$ are shown. For each R, the higher curve corresponds to t→m transition and the lower to m→t transition. Figure 4 shows the relationship between

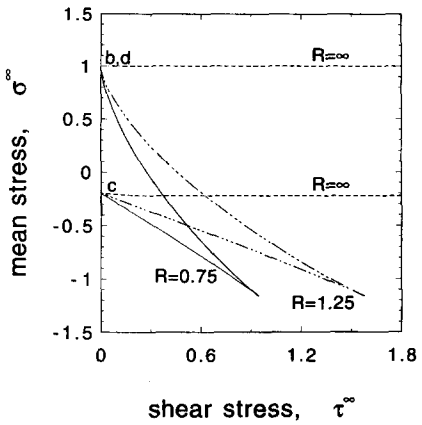

Fig. 3. Stability diagrams in a stress space for different values of R. The diagram is symmetric about $\tau^\infty = 0$. For each R, the higher curve corresponds to t→m transition and the lower to m→t transition. Points b, d, c are the same as in Fig. 4.

far-field mean stress and dilatation in a constrained inclusion for different values of far-field shear stress for $R = 0.75$. To illustrate the hysterisis consider the $\tau^\infty = 0$ curve. The tetragonal phase corresponds to the linear segment ab and the monoclinic phase to the segment cde. If $\sigma^\infty < 1$, then θ stays on the tetragonal branch and reduces back to zero on unloading. At $\sigma^\infty = 1$, tetragonal phase is unstable and θ jumps from b to d and for $\sigma^\infty > 1$ it stays on the monoclinic branch. If σ^∞ decreases monotonically from e, then m→t transition takes place at c.

3. COMPOSITE BEHAVIOUR

In this section we treat ZTC as a dilute composite and study its constitutive behaviour through orientation averaging. Since our interest is in crack propagation, we treat only plane problems.

Consider a ceramic matrix with tetragonal zirconia inclusions. We assume that all inclusions in the body are spherical and randomly oriented with one of the tetragonal planes being the plane under consideration. Consider an inclusion at point (x, y) (see Fig. 5). Let the angle between the tetragonal c axis of the inclusion and the x-axis be β. By our assumption $\beta \in [0, 2\pi]$. Let $x'y'$ be cartesian coordinates with x' parallel to the tetragonal c-axis of the inclusion. Then the far-field mean and shear stresses which trigger the transformation in an inclusion, in non-dimensional form are

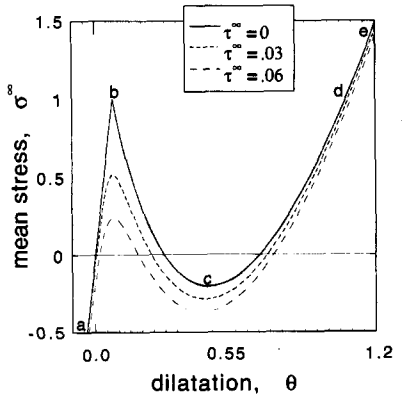

Fig. 4. Far-field mean stress σ^∞ vs dilatation θ of a single constrained inclusion for various values of far-field shear stress τ^∞. Points b, d, c are the same as in Fig. 3.

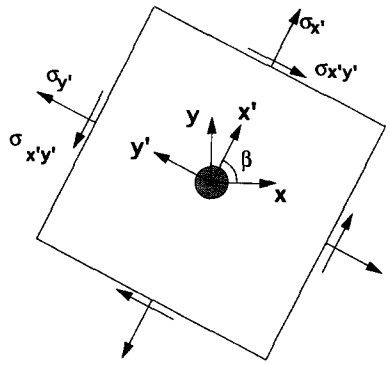

Fig. 5. Far-field stresses on an inclusion (shaded) with orientation β. Cartesian coordinates (x', y', z) are chosen in such a way that x' is parallel to the tetragonal c-axis of the inclusion.

$$\sigma^\infty(x, y) \equiv \frac{1}{3|\tilde{\sigma}^c|}(\sigma_{x'} + \sigma_{y'} + \sigma_z) = \frac{1}{3|\tilde{\sigma}^c|}(\sigma_x + \sigma_y + \sigma_z) \tag{25}$$

$$\tau^\infty(x, y, \beta) \equiv \frac{1}{|\tilde{\sigma}^c|}(\tau_{x'y'}) = \frac{1}{|\tilde{\sigma}^c|} \times \left[-\frac{\sigma_x - \sigma_y}{2} \sin(2\beta) + \tau_{xy} \cos(2\beta) \right]. \tag{26}$$

Notice that $\tau(\beta) = -\tau(\pi/2 + \beta) = \tau(\pi + \beta)$. Since the transformation criterion depends only on $[\tau^\infty]^2$ [see equation (27)], we consider only $\beta \in [0, \pi/2]$.

Let's assume that the constitutive behaviour of a single constrained inclusion is governed by equations (17) and (18) in which σ^∞ and τ^∞ are determined from equations (25) and (26). Now we are in a position to set up a transformation criterion. Since our constitutive model exhibits hysterisis (see Fig. 4), it is necessary to consider the stress history of an inclusion in order to decide if it has transformed. We illustrate the effect of hysterisis by examining the stress histories shown in Fig. 6. The dotted path from A, where the inclusion is in tetragonal phase, to B never crosses the phase boundary, hence the inclusion is still in tetragonal phase at B. On the other path ACB, at $t = t_s$, the inclusion transforms to monoclinic phase. Since the phase boundary in Fig. 6 is the stability limit of the tetragonal phase, there is no reverse transformation at $t = t_f$.

It can be seen from Fig. 6 that for an inclusion to be in monoclinic phase, its stress history must contain points which lie in the shaded region. Using equations

(23) and (24), we find that an inclusion is in monoclinic phase if the far-field stresses acting on it satisfy

$$\sigma^\infty \geq 1, \quad -\infty < \tau^\infty < \infty$$

or

$$1 > \sigma^\infty \geq 0, \quad [\tau^\infty]^2 - [f(\sigma^\infty)]^2 \geq 0 \qquad (27)$$

where we have considered only $\sigma^\infty > 0$, which is sufficient for our purposes. In plane strain the stress history is determined by specifying σ_x, σ_y and τ_{xy} as functions of some parameter t. For an inclusion with orientation β, the stress history determines [through equations (25) and (26)] a loading path like the ones shown in Fig. 6. From equations (25)–(27), we see that the transformation criterion can be expressed as a function of t and β

$$g(t, \beta) \geq 0 \qquad (28)$$

where g is defined as

$$g(t, \beta) = \begin{cases} \sigma^\infty(t) - 1, & \sigma^\infty(t) \geq 1, \\ [\tau^\infty(t, \beta)]^2 - [f(\sigma^\infty(t))]^2, & 1 > \sigma^\infty(t) \geq 0. \end{cases}$$

Now, consider a representative material point of our composite. We assume that it contains zirconia inclusions with all possible orientations, so $\beta \in [0, \pi/2]$. Let m be a subset of $[0, \pi/2]$ and suppose that $\beta \in m(t)$ satisfies inequality (28), i.e.

$$m(t) = \{\beta \in [0, \pi/2] : g(t, \beta) \geq 0\}. \qquad (29)$$

The set $m(t)$ characterises orientations of inclusions in monoclinic phase due to stresses at the current value of t, which means that for all $\beta \in m(t)$ the far-field stresses $[\sigma^\infty(\beta, t), \tau^\infty(\beta, t)]$ lie in the shaded region in Fig. 6. For instance, since all inclusions are in tetragonal phase at $t = -\infty$, the set $m(-\infty)$ is empty. However the set $m(t)$ does not include all monoclinic inclusions. This becomes clear if we consider the stress history ACB of an inclusion shown in Fig. 6, due to which the inclusion transforms at $t = t_s$.

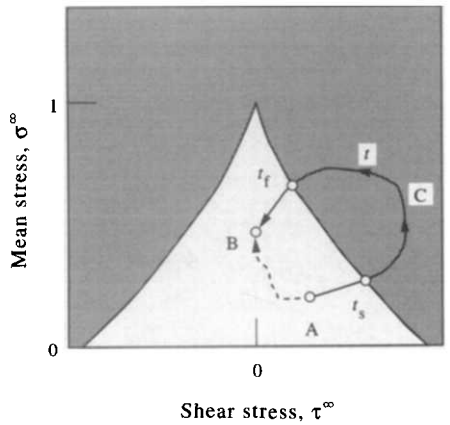

Fig. 6. Schematic illustration of different stress histories of an inclusion (parametrised by t). The shaded region shows where the tetragonal phase is unstable. The loading path ACB causes the inclusion to transform at t_s, whereas the dotted path does not cause it to transform.

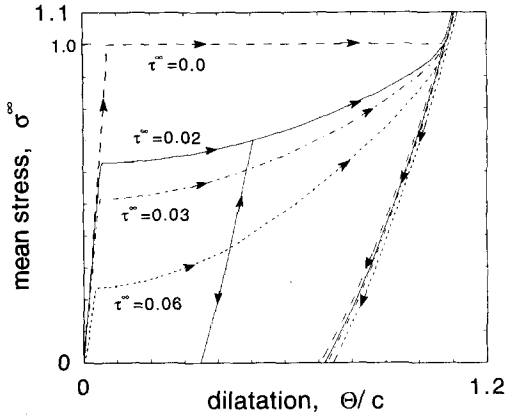

Fig. 7. Stress strain relations for the representative point of the composite. For $\tau^\infty = 0.02$, σ^∞ is increased monotonically from 0 to 0.7, then decreased monotonically from 0.7 to 0 and then increased monotonically from 0 to 1.1 and then decreased monotonically from 1.1 to 0. For all other cases σ^∞ is increased monotonically from 0 to 1.1, then decreased monotonically from 1.1 to 0.

For any $t > t_f$, the far-field stresses on the inclusion do not satisfy inequality (28), but since there is no reverse m→t transformation, the inclusion will still be in monoclinic phase. Accounting for the stress history of inclusions, we find that the orientation of inclusions in monoclinic phase at t is given by

$$\beta \in M(t) = \cup_{s \leq t} m(s). \qquad (30)$$

M is a union of subintervals of $[0, \pi/2]$. The fraction of inclusions in monoclinic phase is given by $2|M|/\pi$, where by $|M|$ we mean the total length of M.

Let the volume fraction of inclusions in our ZTC be c. We define the dilatation $\Theta(x, y)$, to be the average of the dilatation of all inclusions at (x, y). From equation (30) we know that the inclusions in monoclinic phase have orientations $\beta \in M(t)$. Inclusions with orientations $\beta \in [0, \pi/2] \backslash M(t)$ (segment $[0, \pi/2]$ without M) have not yet transformed and are in tetragonal phase. Then by averaging over all orientations present at (x, y) we get

$$\Theta(t) = \frac{2c}{\pi} \int_{M(t)} \theta(t, \beta)\, d\beta + \frac{2c}{\pi} \int_{[0, \pi/2] \backslash M(t)} \theta(t, \beta)\, d\beta. \qquad (31)$$

The first integral corresponds to inclusions in monoclinic phase and the second to inclusions in tetragonal phase. For both integrals $\theta(\beta)$ is obtained by solving equations (17) and (18). We pick $\theta(\beta)$ which lies on the monoclinic branch for the first integral and on the tetragonal branch for the second integral. Let us subject a representative material point of our composite to a fixed shear stress and monotonically changing mean stress and study the dependence of Θ on σ^∞ (see Fig. 7). One can see that for $\tau^\infty = 0$ all inclusions transform at $\sigma^\infty = 1$, hence we have a jump in Θ. For curves with $\tau^\infty \neq 0$, Θ is continuous with σ^∞, because the composite particle can be "partially" transformed.

4. TRANSFORMATION TOUGHENING

In this section we calculate the shape of a transformation zone around a steadily propagating crack and find the resulting transformation toughening. We assume that there is no elastic interaction between inclusions, which is justified only for small transformation strains (see [14]).

Let $\{\bar{x}, \bar{y}, \bar{z}\}$ be the standard dimensional cartesian co-ordinates whose origin lies at the crack tip and suppose that σ_{ij} and ϵ_{ij}, $i, j \in \{\bar{x}, \bar{y}, \bar{z}\}$, are components of stress and strain. Let $\{\bar{r}, \phi, \bar{z}\}$ be polar coordinates such that $\bar{r}^2 = \bar{x}^2 + \bar{y}^2$ and $\phi = \arctan(\bar{y}/\bar{x})$. For plane strain ($\bar{\epsilon}_{\bar{z}\bar{x}} = \epsilon_{\bar{z}\bar{y}} = \epsilon_{\bar{z}} = 0$) the equilibrium stress field, near the crack tip, for mode I cracks can be written as [28]

$$\begin{bmatrix} \sigma_{\bar{x}} \\ \sigma_{\bar{x}\bar{y}} \\ \sigma_{\bar{y}} \end{bmatrix} = \frac{K\cos(\phi/2)}{\sqrt{2\pi\bar{r}}} \begin{bmatrix} 1 - \sin(\phi/2)\sin(3\phi/2) \\ \sin(\phi/2)\cos(3\phi/2) \\ 1 + \sin(\phi/2)\sin(3\phi/2) \end{bmatrix} \tag{32}$$

where the stress intensity factor K depends only on boundary conditions and geometry of the body and

$$\sigma_{\bar{z}} = \nu(\sigma_{\bar{x}} + \sigma_{\bar{y}}) \tag{33}$$

where ν is the Poisson's ratio. We non-dimensionalise lengths as follows

$$x = \frac{\bar{x}}{(K/|\bar{\sigma}^c|)^2}; \quad y = \frac{\bar{y}}{(K/|\bar{\sigma}^c|)^2};$$
$$z = \frac{\bar{z}}{(K/|\bar{\sigma}^c|)^2}; \quad r = \frac{\bar{r}}{(K/|\bar{\sigma}^c|)^2}. \tag{34}$$

Consider an inclusion at point (x, y) whose tetragonal axis makes an angle β with the x-axis (see Fig. 4). Far-field stresses on the inclusion are completely determined by the stress field due to the propagating crack, and are obtained from equations (25), (26), (32) and (33), in non-dimensional form to be

$$\sigma^\infty = \sigma^\infty(x, y) = [2(1+\nu)\cos(\phi/2)]/[3\sqrt{2\pi r}]$$
$$\tau^\infty = \tau^\infty(x, y, \beta) = [\sin\phi\cos(2\beta - 3\phi/2)]/\sqrt{8\pi r} \tag{35}$$

where $r^2 = x^2 + y^2$, $\phi = \arctan(y/x)$.

The stress history of an inclusion, for quasistatic and steady crack propagation in x direction, can be found by decreasing its x coordinate in the stress field around a stationary crack tip. Hence in our case $t = -x$. An example of such a stress history is shown in Fig. 8 juxtaposed with the phase diagram for $R = 0.75$, for inclusions with different orientations β and fixed $y = 0.53$ [Fig. 8(a)] and for inclusions with different values of y and fixed orientation $\beta = 15.6°$ [Fig. 8(b)]. All curves start and end at the stress free state, which corresponds to inclusions being unstressed before the crack tip approaches and after the crack tip passes an inclusion. Notice that once an inclusion transforms, it stays in the monoclinic phase, since the monoclinic phase is at least metastable in the unstressed state.

We refer to the region around a crack where inclusions have transformed as the transformation zone. To find the transformation zone for quasistatic and steady crack propagation, we rewrite the transformation criterion (28) as

$$g(r, \phi, \beta) \geq 0 \tag{36}$$

where g is defined as

$$g(r, \phi, \beta) = \begin{cases} \sigma^\infty(r, \phi) - 1, & \sigma^\infty(r, \phi) \geq 1, \\ \mathrm{d}(r, \phi) + \cos(4\beta - 3\phi), & 1 > \sigma^\infty(r, \phi) \geq 0, \end{cases} \tag{37}$$

and

$$\mathrm{d}(r, \phi) = 1 - \frac{16\pi r}{\sin^2\phi}[f(\sigma^\infty(r, \phi))]^2. \tag{38}$$

We have used the identity $[\tau^\infty(r, \phi, \beta)]^2 - [f(\sigma^\infty(r, \phi))]^2 = \mathrm{d}(r, \phi) + \cos(4\beta - 3\phi)$ [see equations (28) and (35)] in deriving equation (37). We now find $\tilde{m}(r, \phi)$ such that $\beta \in \tilde{m}(r, \phi)$ satisfies inequality (36). First consider the case $1 > \sigma^\infty(r, \phi) \geq 0$. If $\mathrm{d}(r, \phi) < -1$, then $\tilde{m}(r, \phi)$ is the empty set $\emptyset$. If $1 \geq \mathrm{d}(\bar{r}, \phi) \geq -1$, then one can show that inclusions with orientation

$$\beta \in \tilde{m}^*(r, \phi) = \begin{cases} \left[\dfrac{3\phi - \delta(r,\phi)}{4}, \dfrac{3\phi + \delta(r,\phi)}{4}\right], & \dfrac{3\phi - \delta(r,\phi)}{4} \geq 0 \text{ and } \dfrac{3\phi + \delta(r,\phi)}{4} \leq \dfrac{\pi}{2}, \\ \left[0, \dfrac{3\phi + \delta(r,\phi)}{4}\right] \cup \left[\dfrac{\pi}{2} + \dfrac{3\phi - \delta(r,\phi)}{4}, \dfrac{\pi}{2}\right], & \dfrac{3\phi - \delta(r,\phi)}{4} \leq 0 \text{ and } \dfrac{3\phi + \delta(r,\phi)}{4} \leq \dfrac{\pi}{2}, \\ \left[0, \dfrac{3\phi + \delta(r,\phi)}{4} - \dfrac{\pi}{2}\right] \cup \left[\dfrac{3\phi - \delta(r,\phi)}{4}, \dfrac{\pi}{2}\right], & \dfrac{3\phi - \delta(r,\phi)}{4} \geq 0 \text{ and } \dfrac{3\phi + \delta(r,\phi)}{4} \geq \dfrac{\pi}{2}, \\ [0, \pi/2], & \dfrac{3\phi - \delta(r,\phi)}{4} \leq 0 \text{ and } \dfrac{3\phi + \delta(r,\phi)}{4} \geq \dfrac{\pi}{2}, \end{cases} \tag{39}$$

where $\delta = \arccos[-\mathrm{d}(\bar{r}, \phi)]$, satisfy inequality (36). For the case $\sigma^\infty \geq 1$ all inclusions transform and we obtain

$$\tilde{m}(r, \phi) = \begin{cases} [0, \pi/2], & \sigma^\infty(r, \phi) \geq 1, \\ \tilde{m}^{**}, & 1 > \sigma^\infty(r, \phi) \geq 0, \end{cases} \tag{40}$$

where

$$\tilde{m}^{**}(r, \phi) = \begin{cases} \emptyset, & \mathrm{d}(r, \phi) < -1, \\ \tilde{m}^*, & 1 \geq \mathrm{d}(\bar{r}, \phi) \geq -1. \end{cases} \tag{41}$$

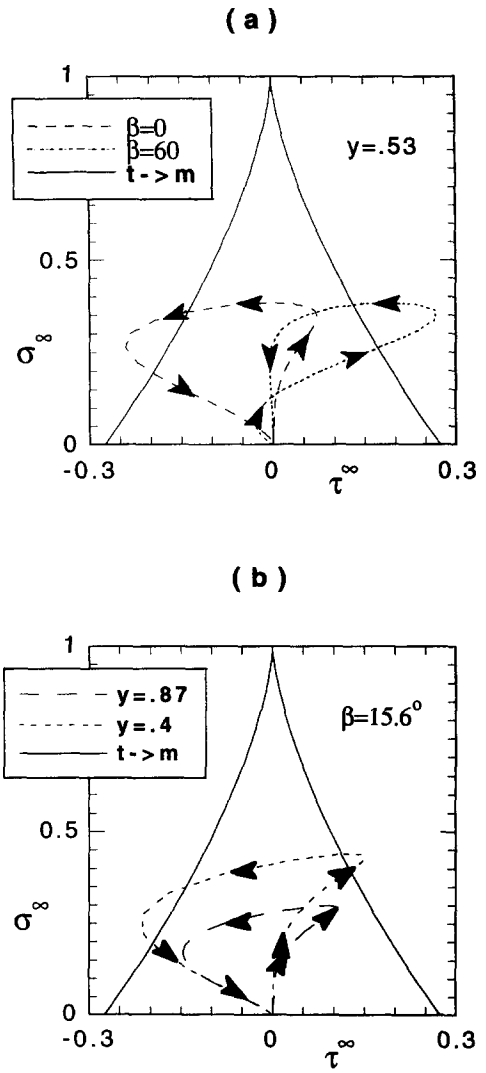

Fig. 8. Far-field stress history due to quasistatic crack propagation of (a) inclusions with different orientations and $y = 0.53$ and (b) inclusions with different values of y and fixed orientation ($\beta = 15.6°$), juxtaposed with the stability diagram ($R = 0.75$).

Now since $r^2 = x^2 + y^2$ and $\phi = \arctan(y/x)$, we get

$$m_y(x) = \tilde{m}[r(x, y), \phi(x, y)]. \tag{42}$$

Using equations (30) and (42), we find that the set of inclusions in monoclinic phase at (x, y) is

$$M(x, y) = \bigcup_{u \geq x} m_y(u) \tag{43}$$

and the fraction of inclusions in monoclinic phase is given by

$$m_f(x, y) = 2|M(x, y)|/\pi. \tag{44}$$

Figure 9 shows level curves of m_f. For $R = \infty$ all inclusions are in monoclinic phase inside the transformation zone, while for $R = 0.75$ there is a large region with partial transformation. For the purely dilatant case $R = \infty$, the height of the region of

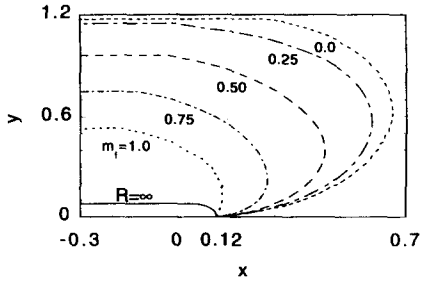

Fig. 9. Level curves of fraction of transformed inclusions m_f. For $R = \infty$ (purely mean stress criterion) $m_f = 1$ on and below the solid line and $m_f = 0$ elsewhere. All the other curves correspond to $R = 0.75$. The crack lies on the negative x-axis with its tip at the origin.

complete transformation, is approximately one fifth of the height of the fully transformed region for the case $R = 0.75$. The gradual decrease in the fraction of transformed inclusions with distance from the crack for $R = 0.75$, agrees qualitatively with the experiments of Marshal *et al.* [29], whereas it decreases abruptly for $R = \infty$. Directly ahead of the crack, since $\tau^\infty = 0$, m_f shows a jump from 1 to 0 at $x = 0.12$ for all R. If the distance ahead of the crack tip where the jump occurs is l, then the critical stress can be estimated from the measurement of l and the relation $\tilde{\sigma}^c = 0.3464\ Kl^{-1/2}$.

Figure 10 shows how the set M of transformed particles changes with x, for a particular $y = 0.53$ and $R = 0.75$. One can see that inclusions with orientation around $\beta = 30°$ are the first to transform at $x \approx 0.63$, while inclusions with orientation around $\beta = 15°$ do not transform until $x \approx -0.17$.

We shall refer to the region behind the crack tip where m_f does not vary with x as the wake. Figure 11 shows the orientation of inclusions that have transformed in the wake as a function of their vertical distance from the crack. For the case $R = 0.75$ we see that all inclusions have transformed for $y \leqslant 0.53$, while only a fraction of inclusions present have transformed from $0.53 < y \leqslant 1.15$ [also see Fig. 8(b)]. We have assumed that inclusions with $\beta \in [0, \pi/2]$ are present at every point. Instead, if we had only inclusions with $\beta \in [53°, 72°]$, then we would have the

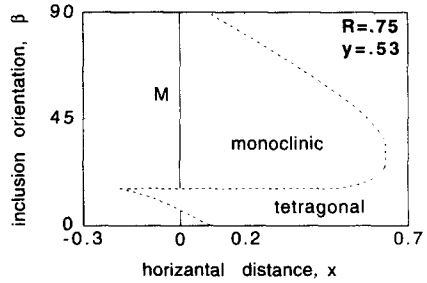

Fig. 10. Evolution of the set of transformed inclusions M with distance from the tip x, for $y = 0.53$ and $R = 0.75$. The crack lies along the negative x-axis with the tip at the origin. The solid vertical line shows the set M at $x = 0$.

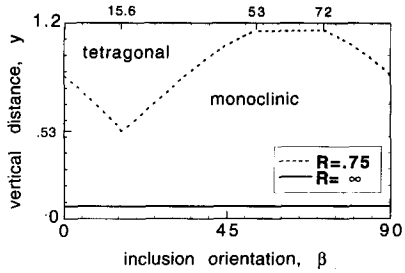

Fig. 11. Orientation of inclusions which have transformed in the wake as a function of their vertical distance from the crack. Transformed inclusions lie below the dotted line for $R = 0.75$ and below the solid line for $R = \infty$.

largest zone of complete transformation and all inclusions would have transformed for $0 < y \leqslant 11.5$. In the case of pure mean stress criterion ($R = \infty$) all inclusions have transformed for $y \leqslant 0.08$.

If an inclusion transforms, then its transformation dilatation $\Delta\theta$ is obtained by subtracting its dilatation before transformation from its dilatation after transformation. Since the far-field stresses on the inclusion with orientation β when it transforms are known, we can solve equations (17) and (18) to obtain θ corresponding to the monoclinic and tetragonal phases. Then the difference between them gives $\Delta\theta(\beta)$. From equation (43), we know that inclusions with orientations $\beta \in M(x, y)$ are in monoclinic phase at (x, y). Thus the transformation dilatation $\Delta\Theta$ at (x, y) in non-dimensional form is

$$\Delta\Theta(x, y) = \frac{2c}{\pi} \int_{M(x,y)} \Delta\theta(\beta)\, \mathrm{d}\beta. \tag{45}$$

Figure 12 shows the variation of $\Delta\Theta$ with distance from the crack y, in the wake for different values of R. For $R = 0.75$ and 1.25 all inclusions have transformed for values of y below the kink, whereas above the kink only a fraction have transformed. In the region with complete transformation, $\Delta\Theta$ is constant only for the case $R = \infty$.

With $\Delta\Theta$ known from equation (45) one can calculate toughening due to transformation dilatation. By considering two circular cylindrical spots (of radius b), located symmetrically with respect to the plane of the crack, one can obtain expressions for the

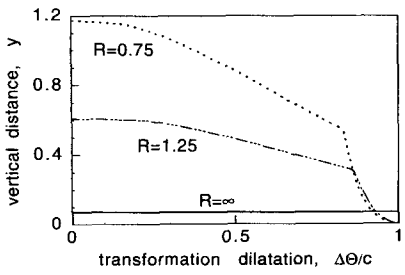

Fig. 12. Variation of transformation dilatation $\Delta\Theta$ with vertical distance from crack y, for different values of R.

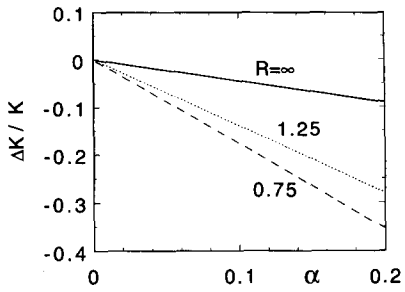

Fig. 13. $\Delta K/K$ vs α for different values of R.

stress intensity factor $\mathrm{d}K$ induced by the spots when they undergo a uniform transformation dilatation (see [13, 21, 30, 31]; since we could not find the derivation of the expression for $\mathrm{d}K$ in the literature, we sketch it in the Appendix). Under conditions of plane strain, if the spots undergo an uniform area dilatation Ω, then the stress intensity factor induced is (A9)

$$\mathrm{d}K = \sqrt{\frac{\pi}{8}} \frac{Eb^2\Omega}{(1-\nu^2)\bar{r}^{3/2}} \cos(\tfrac{3}{2}\phi) \tag{46}$$

where E is the Young's modulus and ν is the Poisson's ratio of the composite and the dimensional $\bar{r} = r(K/|\tilde{\sigma}^c|)^2$. Following the approach of Budiansky *et al.* [14] we obtain an approximation to the area dilatation Ω in the xy plane as

$$\Omega(x, y) = \tfrac{2}{3}(1+\nu)\tilde{\theta}_T \Delta\Theta(x, y). \tag{47}$$

The stress intensity factor at the crack tip is the sum of the applied stress intensity factor K and the stress intensity due to transformed inclusions ΔK ($\Delta K < 0$ corresponds to toughening). One can find toughness induced by the transformed inclusions by integrating equation (46) over the transformation zone. Let $\mathscr{A}$ be the part of a transformation zone above $x = 0$, then

$$\frac{\Delta K}{K} = \alpha \int_{\mathscr{A}} \frac{\Delta\Theta(r, \phi)\cos(\frac{3}{2}\phi)}{cr^{3/2}}\, \mathrm{d}\mathscr{A}. \tag{48}$$

where $\alpha = (Ec\tilde{\theta}_T)/(3\sqrt{2\pi}(1-\nu)\tilde{\sigma}^c)$. In calculating the transformation zone, we had assumed that stresses due to transformation do not affect inclusions, hence we expect equation (48) to be valid only for small α.

We compute the integral in equation (48) and plot $\Delta K/K$ vs α in Fig. 13 for different values of R. For the case of $R = \infty$, the difference between the numerically computed value and the analytical value of -0.45 (from [14]) was less than 1%. It is well known that the experimentally measured ΔK is 2–3 times that predicted by a purely mean stress criterion ($R = \infty$) (see Fig. 43 of [5]). The ratio of ΔK for $R = 1.25$ to ΔK for $R = \infty$ is 3.1, while the ratio of ΔK for $R = 0.75$ to ΔK for $R = \infty$ is 3.9. The overestimation may be due to our neglect of interaction among inclusions and oversimplified treatment of twinning. Neverthe-

less our calculations show that the effect of shear induced transformation on toughness enhancement is profound. So to achieve an agreement between theoretical prediction and measurements, it is essential to take shear stresses into account in the transformation criterion.

5. CONCLUSIONS

We have illustrated how orientation averaging can be used to obtain a non-linear stress strain relation for ZTC. The constitutive model developed here is capable of predicting large transformation zones with gradual decrease of the number of transformed inclusions, observed recently by Marshal *et al.* [29]. We have also shown that both the shape and height of the transformation zone can be varied to increase transformation toughening by controlling the orientation of inclusions. Finally, the prediction of toughening by our criterion, which involves both mean stress and shear stress, agrees well with experiments and is approximately three times that predicted by a purely mean stress criterion. Future work is required for an accurate representation of twinning inside inclusions and for studying elastic interaction between them.

Acknowledgements—This work was supported through grants NSF/DMS 8718881, AFOSR 91-0301, ARO 28987-MA/270 63-MA-SM and ONR N0014-91-J-4034 and by a grant-in-aid assistantship from the Graduate School of the University of Minnesota. We thank R. D. James for valuable discussions.

REFERENCES

1. K. Tsukuma and M. Shimada, *J. Mater. Sci.* **20,** 1178 (1985).
2. A. G. Evans, *J. Am. Ceram. Soc.* **73,** 187 (1990).
3. R. C. Garvie, R. H. J. Hannink and R. T. Pascoe, *Nature* (Lond.) **258,** 703 (1975).
4. A. H. Heuer and A. G. Evans, *J. Am. Ceram. Soc.* **63,** 241 (1980).
5. A. G. Evans and R. M. Cannon, *Acta metall.* **34,** 761 (1986).
6. D. J. Green, R. H. J. Hannink and M. V. Swain, *Transformation Toughening of Ceramics*. CRC Press (1989).
7. E. C. Subbarao, H. S. Maiti and K. K. Srivastava, *Physica status solidi* (a) **21,** 9 (1974).
8. S. Block, J. A. H. Da Jornada and J. G. Piermarini, *J. Am. Ceram. Soc.* **68,** 497 (1985).
9. H. Arashi, T. Yagi, S. Akimoto and Y. Kudoh, *Phys. Rev. B* **41,** 4309 (1990).
10. O. Ohtaka, T. Yamanaka, S. Kume, E. Ito and A. Navrotsky, *J. Am. Ceram. Soc.* **74,** 505 (1991).
11. I.-Wei. Chen and Y.-H. Chiao, *Acta metall.* **33,** 1445 (1985).
12. P. M. Kelly and C. J. Ball, *J. Am. Ceram. Soc.* **69,** 259 (1986).
13. R. M. McMeeking and A. G. Evans, *J. Am. Ceram. Soc.* **65,** 242 (1982).
14. B. Budiansky, J. W. Hutchinson and J. C. Lambropoulos, *Int. J. Solids Struct.* **19,** 337 (1983).
15. L. R. F. Rose, *Proc. R. Soc. Lond. A* **412,** 169 (1987).
16. H. Okada, T. Tamura, N. Ramakrishnan, S. N. Atluri and J. S. Epstein, *Acta metall.* **40,** 1421 (1992).
17. I.-Wei. Chen, *J. Am. Ceram. Soc.* **74,** 2564 (1991).
18. I.-Wei. Chen and P. E. Reyes-Morel, *J. Am. Ceram. Soc.* **69,** 181 (1986).
19. P. E. Reyes-Morel and I.-Wei. Chen, *J. Am. Ceram. Soc.* **71,** 343 (1988).
20. J. C. Lambropoulos, *Int. J. Solids Struct.* **22,** 1083 (1986).
21. D. M. Stump, *Phil. Mag. A* **64,** 879 (1991).
22. B. Budiansky and L. Truskinovsky, *J. Mech. Phys. Solids* **41,** 1445 (1993).
23. B. Budiansky and S. B. Batdorf, A mathematical theory of plasticity based on the concept of slip, NACA Technical Note No. 1871 (1949).
24. A. Lagzdiņš, V. Tamužs, G. Teters and A. Krēgers. *Orientation Averaging in Mechanics of Solids*. Longman Scientific and Technical (1992).
25. J. D. Eshelby, *Proc. R. Soc. Lond. A* **241,** 376 (1957).
26. R. Hill, *J. Mech. Phys. Solids* **13,** 89 (1965).
27. R. E. Cohen, M. J. Mehl and L. L. Boyer, *Physica B* **150,** 1 (1988).
28. J. Rice, *Fracture* (edited by H. Liebowitz), Vol. 2., Chap. III. Academic Press, New York (1968).
29. D. B. Marshal, M. C. Shaw, R. H. Dauskardt, R. O. Ritchie, M. J. Readey and A. H. Heuer, *J. Am. Ceram. Soc.* **73,** 2659 (1990).
30. J. W. Hutchinson, On steady quasi-static crack growth, Harvard University Report (DEAP S-8) (1974).
31. N. K. Simha, Ph.D. thesis, Univ. of Minnesota (1994).
32. N. I. Muskhelishvili, *Some Basic Problems of the Mathematical Theory of Elasticity*, 3rd edn. Noordhoff, Groningen (1953).

APPENDIX

Let $\varphi(z)$ and $\psi(z)$ be the Muskhelishvili functions [32] of complex variable z for plane isotropic elasticity such that

$$\sigma_x + \sigma_y = 2(\varphi' + \overline{\varphi'}), \tag{A1}$$

$$\sigma_y - i\sigma_{xy} = \varphi' + \overline{\varphi'} + z\overline{\varphi''} + \overline{\psi'}, \tag{A2}$$

where $' \equiv \mathrm{d}/\mathrm{d}z$ and $\bar{z}$ is the conjugate of z. The stress functions φ and ψ for the problem where two circular spots of radius b, located at z_0 and $\bar{z}_0$, undergo a uniform area dilatation Ω in the presence of a semi-infinite crack (at $y = 0$, $x < 0$), can be considered to be the superposition of the following two problems: (1) The two spots undergo a uniform area dilatation Ω in an infinite plane [resulting in stresses $\hat{\sigma}_x(x) = 0$ (symmetry), $\hat{\sigma}_y(x)$ and $\hat{\sigma}_{xy}(x)$ on the line $y = 0$, $x < 0$]. (2) The faces of a crack which lies at $y = 0$, $x < 0$ are subjected to stresses $-\hat{\sigma}_y(x)$ and $-\hat{\sigma}_{xy}(x)$.

For a complex function $p(z)$, let $p^*(z) = \overline{p(\bar{z})}$. In case (1) by assuming plane stress and by requiring continuity of tractions and displacement across the boundary of the spots, we obtain the stress functions outside the spots as

$$\varphi_1 = 0 \quad \text{and} \quad \psi_1 = \psi_0 + \psi_0^*, \quad |z - z_0| > b \tag{A3}$$

where

$$\psi_0 = -\frac{E\Omega b^2}{4(z - z_0)}$$

and E is the Young's modulus. We then compute

$$\hat{\sigma}_y - i\hat{\sigma}_{xy} = \frac{E\Omega b^2}{4}\left[\frac{1}{(\bar{z} - \bar{z}_0)^2} + \frac{1}{(\bar{z} - z_0)^2}\right].$$

Case (2) leads to the Hilbert problem (see [32]), the solution for which has been written in a convenient form by Rice [28] as

$$\varphi_2' = \frac{1}{2\pi\sqrt{z}} \int_{-\infty}^{0} [\hat{\sigma}_y - i\hat{\sigma}_{xy}]\sqrt{-t}\,\frac{\mathrm{d}t}{t - z} \tag{A4}$$

$$\psi_2' \equiv -z\varphi_2''. \tag{A5}$$

Evaluating the integral in first of equations (A4) by the method of residues we obtain

$$\varphi_2 = p + p^* \tag{A6}$$

$$p' = -\frac{\psi_0'}{2} + \frac{\pi E b^2 \Omega (z + z_0)}{16\pi\sqrt{zz_0}(z - z_0)^2} \tag{A7}$$

Hence the solution to the full problem can be obtained by superposition from equations (A3)–(A7) to be

$$\varphi = \varphi_2$$

$$\psi = \psi_1 + \psi_2. \tag{A8}$$

These expressions agree with the solution given by Hutchinson [30]. The stress intensity factor is obtained from its definition to be

$$dK = \lim_{x \to 0} \sqrt{2\pi x}\sigma_y(x, 0) = \sqrt{\frac{\pi}{8}} \frac{E b^2 \Omega}{\bar{r}^{3/2}} \cos(\tfrac{3}{2}\phi) \tag{A9}$$

where the dimensional $\bar{r}$ and ϕ are obtained from the relation $z = \bar{r}\, e^{i\phi}$. To obtain the stress intensity factor for plane strain, we replace E with $E/(1 - \nu^2)$ where ν is the Poisson's ratio.